Appendix D:

Xu, F., El-Leathy, A.M. and Faeth, G.M. (2000) "Soot Oxidation in Laminar Hydrocarbon/Air Diffusion Flames at Atmospheric Pressure," *Combust. Flame*, submitted.

SOOT OXIDATION IN HYDROCARBON/AIR DIFFUSION FLAMES AT ATMOSPHERIC PRESSURE

F. Xu , A.M. El-Leathy and G. M. Faeth*
Department of Aerospace Engineering
The University of Michigan
Ann Arbor, MI 48109-2140, U.S.A.

Soot oxidation was studied experimentally in laminar hydrocarbon/air diffusion flames at atmospheric pressure. Measurements were carried out along the axes of round jets burning in coflowing air considering acetylene, ethylene, proplyene and propane as fuels. Measurements were limited to the initial stages of soot oxidation (carbon consumption less than 70%) where soot oxidation mainly occurs at the surface of primary soot particles. The following properties were measured as a function of distance above the burner exit: soot concentrations by deconvoluted laser extinction, soot temperatures by deconvoluted multiline emission, soot structure by thermophoretic sampling and analysis using Transmission Electron Microscopy (TEM), concentrations of stable major gas species (N_2, H_2O, H_2, O_2, CO, CO_2, CH_4, C_2H_2, C_2H_4, C_2H_6, C_3H_6, and C_3H_8) by sampling and gas chromatography, concentrations of some radical species (H, OH, O) by the deconvoluted Li/LiOH atomic absorption technique and flow velocities by laser velocimetry. It was found that soot surface oxidation rates are not particularly affected by fuel type for laminar diffusion flames and are described reasonably well by the OH surface oxidation mechanism with a collision efficiency of 0.10, (standard deviation of 0.07) with no significant effect of fuel type in this behavior; these findings are in good agreement with the classical laminar premixed flame measurements of Neoh et al. (1980). Finally, direct rates of surface oxidation by O_2 were small compared to OH oxidation for present conditions, based on estimated O_2 oxidation rates due to Nagle and Strickland-Constable (1962), because soot

*Corresponding author. E-mail: gmfaeth@umich.edu

oxidation was completed near the flame sheet where O_2 concentrations were less than 1.2% by volume.

NOMENCLATURE

C_i	mass of carbon oxidized per mole of species i reacted
d	fuel port exit diameter (m)
d_p	mean primary soot particle diameter (m)
f_s	soot volume fraction (-)
Fr	burner exit Froude number (-), $u_o^2/(gd)$
g	acceleration of gravity (ms^{-2})
[i]	molar concentration of species i (kmole m^{-3})
k	Boltzmann constant (J $molecule^{-1}K^{-1}$)
M_i	molecular weight of species i (kg $kgmol^{-1}$)
n_p	number of primary particles per unit volume (m^{-3})
Re	burner exit Reynolds number (-), $u_o d/\nu_o$
S	soot surface area per unit volume (m^{-1})
t	time (s)
T	temperature (K)
u	streamwise velocity (ms^{-1})
$\bar{v}_i$	mean molecular velocity of species i (ms^{-1})
w_{ox}	soot surface oxidation rate (kg $m^{-2}s^{-1}$)
z	streamwise distance (m)

Greek Symbols

η_i	collision efficiency of species i
ν	kinematic viscosity (m^2s^{-1})

ρ gas density (kg m^{-3})

ρ_s soot density (kg m^{-3})

ϕ fuel-equivalence ratio

Subscripts

o burner exit condition

INTRODUCTION

Soot is an important unsolved problem of combustion science because it is present in most hydrocarbon-fueled flames and current understanding of the reactive and physical processes of soot in flame environments is limited. In particular, lack of knowledge about soot formation and oxidation in flames affects progress toward developing reliable predictions of flame radiation properties, reliable predictions of flame pollutant emission properties and robust methods of computational combustion, among others. Motivated by these observations, the present investigation extended past experimental studies of soot formation in laminar premixed and diffusion flames in this laboratory [1-9], to consider soot oxidation in laminar diffusion flames using similar methods.

Potential soot oxidants in hydrocarbon-fueled diffusion flames include O_2, CO_2, H_2O, O and OH. Numerous simplified treatments have been reported that can be used to estimate soot oxidation rates in frequently-encountered instances when local radical concentrations are not known [10-18]. Present emphasis, however, is on a more fundamental treatment of soot oxidation by considering mechanisms that include potential contributions from both stable and radical species.

The results of the classical study of the oxidation of pyrolytic graphite by O_2, due to Nagle and Strickland-Constable [10], have been shown to be effective for the oxidation of soot by O_2, as well, based on later work by Radcliffe and Appleton [13] and Park and Appleton [14]. Subsequent work by Fenimore and Jones [19] and Mulcahy and Young [20], however, showed that soot oxidation rates in flame environments having relatively small O_2 concentrations substantially exceeded estimates based on the results of Nagle and Strickland-Constable [10], prompting suggestions that radicals such as O and particularly OH might be strong contributors to soot oxidation for such conditions. Neoh and coworkers [21-23] subsequently carried out measurements of soot oxidation in premixed flames to address this issue and provided well documented evidence that OH was the principle oxidant of soot for near-stoichiometric flame conditions (with O_2 mole fractions smaller than 5%), they also found an OH collision efficiency of 0.13 for oxidation when accounting for the actual structure of soot particles as aggregates of primary particles. Later studies by Wicke et al. [24,25] and Roth et al. [26] of soot oxidation in homogeneous environments confirmed the findings of Neoh and coworkers [21-23] within experimental uncertainties.

Due to the importance of soot within diffusion flames for most practical applications, there have been several recent investigations of soot oxidation in laminar diffusion flames. This has included measurements of soot oxidation in round methane/air coflowing jet diffusion flames due to Garo et al. [27,28], in round ethylene/air coflowing jet diffusion flames due to Puri et al. [29,30], and in ethylene-nitrogen/oxygen-argon Wolfhard-Parker burner flames due to Haudiquert et al. [31]. These studies supported the dominant role of OH in the mechanism of soot oxidation within diffusion flames, however, observations of OH collision efficiencies for soot were not in good agreement with the earlier results from premixed flames, e.g., Garo et al. [27,28] observed values of 0.012-0.094 that generally *increased* with increasing temperature, Puri et al. [29,30] observed values of 0.03-0.15 that generally *decreased* with increasing

temperature, and Haudiquert et al. [31] observed values of 0.01-0.11 that generally *decreased* with increasing temperature. One explanation for these discrepancies is that optical scattering and extinction measurements were used to infer soot structure properties during these studies, based on models that have not been very successful for representing the optical properties of soot [32,33]. Supporting this view is that use of similar methods during early studies of soot growth in fuel-rich premixed flames has proved to be problematical, see Xu et al. [4,5] and references cited therein. Whatever the source of the problem, however, these differences between observations of soot oxidation in premixed and diffusion flames clearly must be resolved.

Based on the preceding review of the literature, the present investigation sought to contribute to better understanding of soot oxidation properties in laminar diffusion flames with the following specific objectives: (1) to complete measurements of soot properties (soot volume fraction and primary particle diameters) and flame structure properties (temperature, stable and radical species concentrations, and velocities) within the soot oxidation region of several laminar hydrocarbon-fueled diffusion flames, and (2) to exploit the new measurements to evaluate potential soot oxidation mechanisms, particularly emphasizing the classical approach of Neoh and coworkers [21-23]. The experiments were limited to measurements along the axes of laminar coflowing jet diffusion flames burning in air at atmospheric pressure and fueled with various hydrocarbons, similar to the flames used by Xu and coworkers [7,9] to study soot formation in laminar diffusion flames. The particular hydrocarbon fuels considered included those used by Sunderland and coworkers [1-3] during early studies of soot formation in laminar diffusion flames, e.g., acetylene, ethylene, propylene and propane. Present considerations were limited to the early stages of soot oxidation (carbon consumption less than 70%) where reaction at the surface of primary soot particles dominates the process, rather than the later stages where particle porosity and internal oxidation of the particles become important as discussed by Neoh

et al. [23]. Finally, the following description of the research is brief, more details and a complete tabulation of the measurements are provided by Xu and coworkers [8,9].

EXPERIMENTAL METHODS

The test apparatus and instrumentation were unchanged from the earlier study of soot formation in laminar diffusion flames [7] and will be described only briefly. The test flames were produced by a flat honeycomb burner with an air coflow. The honeycomb burner had 1 mm cell sizes, that were 20 mm long. The burner consisted of a 35 mm diameter inner port for the fuel-containing stream and a 60 mm diameter coannular outer port for the air coflow, both directed vertically upward. The combustion products were removed using a blower which had an inlet diameter of 125 mm located roughly 800 mm above the burner exit. The flames burned in room air with room disturbances controlled by surrounding the flames with several layers of screens and a plastic enclosure. The burner could be traversed in the vertical and horizontal directions to accommodate rigidly-mounted optical instrumentation.

Soot volume fractions were found by deconvoluting laser extinction measurements at 632.8 mm for chord-like paths through the flames, using the refractive indices of Dalzell and Sarofim [34] that have recently been confirmed by Krishnan et al. [35]; experimental uncertainties (95% confidence) of these measurements are estimated to be less than 10% for soot volume fractions greater than 0.02 ppm, increasing inversely proportional to the soot volume fraction for smaller values. Soot temperatures were found by deconvoluting spectral radiation intensities for chord-like paths through the flames and computing temperatures from measurements at wavelength pairs of 550/700, 550/750, 550/830, 600/700, 600/750, 600/830 and 650/750 nm; temperature differences between the average and any of the line pairs were less than 50-100 K and experimental uncertainties (95% confidence) of these measurements were less than 50 K. Concentrations of major gas species were measured using isokinetic sampling and

analysis by gas chromatography, seeking concentrations of N_2, H_2O, H_2, O_2, CO, CO_2, CH_4, C_2H_2, C_2H_4, C_2H_6, C_3H_6, C_3H_8 and neon (the last being a tracer gas used to estimate effects of radial diffusion of lithium-containing species that were used to find H concentrations); experimental uncertainties (95% confidence) of these measurements are estimated to be less than 5%. Soot primary particle diameters were measured using thermophoretic sampling and analysis by Transmission Electron Microscopy (TEM). Primary particles were nearly monodisperse at given positions in each flame (standard deviations were less than 10%) with experimental uncertainties (95% confidence) of the mean diameters estimated to be less than 10%. Streamwise gas velocities were measured using laser velocimetry; experimental uncertainties (95% confidence) of these measurements were estimated be less than 5%. Finally, H concentrations were measured using the Li/LiOH atomic absorption method similar to Neoh and coworkers [21-23] which involved deconvoluted atomic absorption measurements with corrections for radial diffusion of lithium-containing species, as discussed earlier. Corresponding measurements of H concentrations in a methane/oxygen premixed flame were used to calibrate the H concentration measurements as discussed by Xu and Faeth [6]. Experimental uncertainties (95% confidence) of the H concentration measurements are estimated to be less than 30%. Given measured concentrations of H, O_2, H_2 and H_2O, values of O and OH concentrations were computed assuming partial equilibrium among these species following Neoh et al. [21,22] using equilibrium constant data from Chase et al. [36]. This involved finding O and OH concentrations assuming partial equilibrium considering H, H_2O and H_2 concentrations for fuel-rich conditions and H, H_2O and O_2 concentrations for fuel-lean conditions. The laminar premixed flame used to calibrate the H concentration measurements operated using the fuel port of the present burner, see Xu and Faeth [6] for a summary of the properties of this flame.

The present test flames consisted of three acetylene-nitrogen/air laminar jet diffusion flames, that were identical to those considered during the earlier soot formation study [7], and three new flames involving hydrocarbons other than acetylene, e.g., ethylene/air, propylene-nitrogen/air and propane/air flames. Nitrogen dilution of the fuel stream was used to limit maximum soot concentrations in the flames to values less than 2 ppm, in order to avoid measurement problems due to the presence of large soot concentrations.

The general operating properties of all six test flames are summarized in Table 1. A dark-field photograph of one of the flames (Flame 4, the ethylene/air flame) appears in Fig. 1; it is similar in appearance to the other flames. Similar to the flame illustrated in Fig. 1, all the flames were steady and attached close to the honeycomb at the burner exit. The flames generally were yellow due to luminosity from hot soot particles. The luminous flame length (see Table 1) was generally relatively close to the stoichiometric flame length (where the local fuel-equivalence ratio was unity along the flame axis) but was slightly shorter than the stoichiometric flame length for the acetylene-nitrogen/air flames (due to early burn out of soot at fuel-rich conditions) and slightly longer than the stoichiometric flame length for flames fueled with the other hydrocarbons (due to delayed burn out of soot at fuel-lean conditions). Present measurements were confined to the soot oxidation region of the test flames which was located at fuel-rich conditions for all the present flames. The stoichiometric flame temperatures in Table 2 were found from adiabatic combustion calculations using the algorithm of McBride et al. [37]. Finally, potential problems of acetone contamination of acetylene, noted by Hamins et al. [38] and Colket et al. [39,40] are not thought to be a problem for present measurements, as discussed by Xu and Faeth [7].

RESULTS AND DISCUSSION

Flame Structure

Typical TEM photographs of soot samples collected from the present flames are illustrated in Fig. 2. These results were obtained along the axis of the same flame as Fig. 1 (Flame 4, the ethylene/air flame). Images of soot aggregates are provided near the start of foot formation (z = 20 mm), near the maximum soot concentration condition (z = 50 mm) and near the end of soot oxidation (z = 70 mm).

The present soot particles were similar to soot observed during past studies within laminar premixed and diffusion flames, see Refs. 1-5, 7 and 8 and references cited therein, for other examples. The soot particles consisted of roughly spherical primary particles having nearly constant diameters at a given flame condition. The primary particles were collected into open-structured aggregates that are known to be fractal aggregates based on earlier work, see Köylü and Faeth [32] and references cited therein. The aggregates had widely varying numbers of primary particles per aggregate with the average number of primary particles per aggregate progressively increasing with increasing distance from the burner exit. Present test conditions were limited to maximum amounts of soot oxidation of 70% by mass, based on the maximum primary particle diameter observed in each flame. Observations farther into the soot oxidation region yielded significantly reduced aggregate sizes as soot aggregates begin to break up near the end of the soot oxidation process. It should also be noted that present levels of soot oxidation were significantly smaller than conditions where Neoh et al. [21-23] observed effects of porous primary particles, internal soot oxidation, and soot aggregate breakup; therefore, oxidation of soot at the surface of primary particles dominated present observations.

Measurements of gas (soot) temperatures, streamwise gas velocities, soot volume fractions, soot primary particle diameters, the concentrations of major gas species (N_2, H_2, H_2O, O_2, CO, CO_2, CH_4, C_2H_2, C_2H_4, C_2H_6, C_3H_6 and C_3H_8) and the concentrations of radical species (H, O, OH) are plotted as a function of height above the burner exit for typical diffusion flames for each fuel in Figs. 3-6 (Flames 1, 4, 5 and 6), see Ref. 7 for similar results for Flames 2 and 3. Corresponding residence times, found by integrating velocity measurements, are indicated at the top of the plots; these times are relative to the first position where detectable soot volume fractions were observed (at roughly z = 10 mm). Finally, in instances where the measurements extended beyond the flame sheet, the position of the flame sheet, is marked on the figures for reference purposes.

Gas (soot) temperatures in Figs. 3-6 reach a maximum in the soot formation region, somewhat before the flame sheet is reached. Thus, temperatures within the soot oxidation region either remain roughly constant or decrease slightly. Present temperatures at the flame sheet are smaller than the stoichiometric temperatures summarized in Table 1. These trends are similar to earlier observations of acetylene-nitrogen-fueled diffusion flames burning in air [1,7]. This behavior is caused by significant effects of continuum radiation heat losses from soot in these flames [1-3].

Gas velocities in Figs. 3-6 increase with increasing distance from the burner exit due to effects of buoyancy, e.g., velocities increase from burner exit values of 0.003-0.03 m/s to values in excess of 2 m/s at the highest position that was measured. This causes a corresponding stretching of the elapsed time scale at the top of the figures with increasing distance from the burner exit.

As discussed by Xu and Faeth [7], soot formation and oxidation proceed at the same time and the boundary between these two regions is not abrupt. A reasonable definition of this boundary, mentioned earlier, is the point where the soot volume fraction reaches a maximum because soot formation and oxidation dominate soot processes before and after these conditions, respectively. The results in Figs. 3-6 indicate that this boundary is generally reached before the flame sheet is reached. For fuels other than acetylene, the original fuel disappears relatively close to the burner exit and concentrations of acetylene build up rapidly; as a result, concentrations of acetylene are rather similar for flames fueled with acetylene and with the other hydrocarbon fuels. Thus, similar to earlier observations of acetylene-fueled diffusion flames [1,7], the maximum soot volume fraction condition is reached when concentrations of acetylene become small (e.g., when acetylene mole fractions are smaller than 1%).

Results illustrated in Figs. 3-6 show that primary soot particle diameters reach a maximum relatively early in the soot formation region. This behavior occurs because soot growth maintains relatively rapid rates at temperatures smaller than those required for rapid rates of soot nucleation as noted by Tesner [41,42]; this behavior is discussed in earlier studies of soot processes in diffusion flames [1-3,7].

Concentrations of major stable gas species — N_2, CO_2 and H_2O — are seen to be relatively uniform in the soot oxidation region for the results illustrated in Figs. 3-6. This occurs for N_2 because its large concentration in the ambient air causes it to dominate the flame composition. This behavior is also consistent with simple classical ideas about the structure of diffusion flames, where the concentrations of the stable combustion products — CO_2 and H_2O — should reach a maximum at the flame sheet. Also in agreement with classical ideas about the structure of diffusion flames, the concentrations of fuel-like species – C_2H_2, CO, H_2, CH_2, C_2H_4, C_2H_6, C_3H_6, C_8H_8 — all tend to decrease with increasing distance from the burner exit as fuel

oxidation proceeds. In the same manner, concentrations of O_2 progressively increase with increasing distances from the burner exit. Unlike classical diffusion flames, however, fuel-like species penetrate well into the fuel-lean region and the fundamental oxidizing species, O_2, penetrates well into the fuel-rich region, due to finite rate chemistry effects of dissocation, effects of preferential diffusion, and phenomena associated with the formation and oxidation of soot.

Concentrations of radical species illustrated in Figs. 3-6 are of interest due to the role these species play in soot formation and oxidation. Concentrations of H remain relatively constant throughout the soot oxidation region. Thus, unlike laminar premixed flames where acetylene concentrations are relatively constant and soot formation ends due to reduced H concentrations as the flame gases cool, for the present diffusion flames where H concentrations are relatively constant, soot formation ends due to reduced acetylene concentrations as the flame becomes leaner. Other radical species illustrated in Figs. 3-6 are all potential soot oxidizing species — O and OH — and concentrations of both tend to increase with increasing distance from the burner exit; this behavior is mainly driven by increasing concentrations of O_2 in the presence of nearly constant H_2 and H concentrations as the flow becomes leaner.

Additional information about radical concentrations in the present flames is presented in Figs. 7 and 8 where superequilibrium ratios of H, O and OH are plotted as a function of distance from the burner exit for the acetylene-fueled and the other hydrocarbon-fueled flames, respectively. For reference purposes, fuel-equivalence ratios are also plotted on the figures. As a result of partial equilibrium requirements, superequilibrium ratios of H and OH are identical (Even the actual concentrations of these two radicals are not very different in the present flames, see Figs. 3-6). Near the start of the soot formation region (at z = 20 mm), concentrations of H, OH and O are either near or somewhat below equilibrium levels. Subsequently, superequilibrium ratios of all three radicals increase with increasing distance from the burner

with OH and H concentrations yielding superequilibrium ratios of 6-20 throughout most of the soot formation and oxidation regions. Superequilibrium ratios of O are even larger than the rest, continuously increasing with increasing streamwise distance to reach values of 100-1000 near the downstream end of the soot-containing region (or the downstream end of the present measurements). Actual concentrations of H and OH, however, generally are significantly larger than actual concentrations of O throughout most of the soot formation and oxidation regions, with concentrations of the three radicals only becoming comparable near the downstream end of the soot-containing region, see Figs. 3-6. This behavior differs substantially from the soot formation regions of premixed flames where near-equilibrium levels of radical concentrations are observed throughout [6]. Thus, the larger superequilibrium concentrations of H are responsible for the larger rates of soot growth in diffusion flames than in premixed flames for similar temperatures and acetylene concentrations [1,2] through the HACA mechanism [7]. Similarly, larger superequilibrium concentrations of OH also give rise to the possibility that oxidation of soot in diffusion flames may be dominated by reaction with OH, as suggested by Fenimore and Jones [19], Mulcahy and Young [20] and Neoh and coworkers [21-23], rather than by oxidation by O_2.

Soot Oxidation Rate Properties

Present measurements were exploited to study soot oxidation by modifying methods used during earlier studies of soot growth [4,5,7]. Major assumptions were similar to Refs. 4, 5 and 7, as follows: soot oxidation occurred only at the surface of primary soot particles, effects of thermophoresis and diffusion (Brownian) on soot motion are small so that soot particles convect on the local gas velocity, soot density is constant, and the surface area available for soot oxidation is equivalent to constant diameter spherical particles that meet at a point. Present

measurements were confined to the axis of the flames so that variations of soot properties as a function of time could be obtained directly from the elapsed time determinations illustrated in Figs. 3-6.

Properties that must be known to find soot oxidation rates include the number of primary particles per unit volume, n_p, the soot surface area per unit volume, S, and the mass of soot oxidized per unit soot surface area and time w_{ox}. The number of primary particles per unit volume was obtained from the measured soot volume fraction and primary particle diameter, as follows:

$$n_p = 6f_s/(\pi d_p^3) \tag{1}$$

with experimental uncertainties (95% confidence), of n_p estimated to be less than 32% for $f_s >$ 0.1 ppm. The soot surface area per unit volume can be obtained from the same measured properties, as follows:

$$S = \pi d_p^2 n_p = 6f_s/d_p \tag{2}$$

where the last equality follows from Eq. 1; the experimental uncertainties (95% confidence) of S are estimated to be less than 15% for $f_s > 0.1$ ppm. Finally, conservation of soot mass along a streamline under the present assumptions yields an expression for the soot oxidation rate per unit surface area, w_{ox}, as follows:

$$w_{ox} = -(\rho/S)d(\rho_s f_s/\rho)dt \tag{3}$$

where S is found from Eq. 2 and the minus sign is inserted so that w_{ox} is a positive number. The gas density in Eq. 3 was found from measurements of gas species concentrations and temperatures, assuming an ideal gas mixture and neglecting the small volume of soot for present conditions. The soot density in Eq. 3 was taken to be equal to 1850 kg/m^3, similar to past work

[1-5,7]. The temporal derivatives in Eq. 3 were found from three-point least-squares fits of the argument of the derivative, $\rho_s f_s/\rho$, which also is similar to past work [1-5,7].

The three derived soot oxidation properties — S, n_p and w_{ox} — are plotted as a function of distance along the axes of the acetylene-fueled and other hydrocarbon-fueled flames in Figs. 9 and 10, respectively. These results generally are limited to the region of the flames dominated by soot oxidation. The soot surface area per unit volume tends to vary similar to soot volume fraction, tending to decrease with increasing streamwise distance, within the soot oxidation region.

The number of primary particles per unit volume plotted in Figs. 9 and 10 tend to vary similar to S but exhibit more scattered behavior due to the larger experimental uncertainties of n_p than the other variables illustrated in Figs. 9 and 10. Soot nucleation rates become small with increasing distance into the soot oxidation region, see the results in Ref. 8 for acetylene-fueled diffusion flames; then continued mixing of the flow combined with effects of soot oxidation causes n_p to decrease with increasing distance from the burner exit for most of the flames. In particular, this behavior is just beginning to appear when present measurements ended for flame 3.

Soot oxidation rates illustrated in Figs. 9 and 10 tend to increase with increasing streamwise distance throughout the soot oxidation region. This trend is reasonable because the concentrations of all the species thought to be responsible for soot oxidation — O_2, CO_2, H_2O, O and OH — all increase as the distance from the burner exit increases, see Figs. 4-6.

Soot Surface Oxidation

Present measurements of soot oxidation were corrected for effects of soot growth using the expression based on the Colket and Hall [43] soot growth mechanism as correlated for both premixed and diffusion flame environments by Xu et al. [4,5,7]. No condition is considered in the following, however, where the correction for soot growth was more than half the soot oxidation rate.

Similar to Neoh et al. [21,22], present soot oxidation rates (corrected for soot growth) were converted into collision efficiencies (or reaction probabilities) based on kinetic theory estimates of the collision rates of a given gas species with the surfaces of primary soot particles. Thus, the collision efficiency, η_i, for a potential oxidizing species, i, is given by the following expression [2]:

$$\eta_i = 4w_{ox}/(C_i[i]\bar{v}_i) \tag{4}$$

where C_i is the mass of carbon removed from the surface per mole of species i reacting at the surface, [i] is the gas phase concentration of i adjacent to the surface, and

$$\bar{v}_i = (8kT/(\pi M_i))^{1/2} \tag{5}$$

is the (Boltzmann) equilibrium mean molecular velocity of species i. In the following, values of the η_i will be considered for potential soot oxidation by O_2, CO_2, H_2O, O and OH, in turn.

The collision efficiencies of O_2 for soot oxidation are plotted as a function of height above the burner in Fig. 11. Results shown on the figure include the range of values observed by Neoh et al. [21,22] in premixed flames, the values determined from the present experiments in diffusion flames, and values estimated from the predictions of Nagle and Strickland-Constable

[10] for the conditions where present observations were made in diffusion flames. The Nagle and Strickland-Constable [10] approach has exhibited effective capabilities to predict soot oxidation by O_2 and there are significant levels of O_2 along the present soot paths, see Figs. 3-6. Thus, the fact that the Nagle and Strickland-Constable estimates of the O_2 collision efficiency are 10-100 times smaller than the present measurements strongly suggests that some other species is mainly responsible for soot oxidation in the present flames. Other evidence that O_2 is not the main direct soot oxidizing species for flame environments is provided by the large scatter (nearly a factor of 100) of the present collision efficiencies for diffusion flames combined with the even larger scatter (more than a factor of 100) of the O_2 collision efficiencies of Neoh et al. [21] in premixed flames.

The collision efficiencies of CO_2 for soot oxidation are plotted as a function of height above the burner in Fig. 12. Results shown on the figure include the range of values observed by Neoh et al. [21] in premixed flames, and values from the present investigation in diffusion flames both considering and ignoring the contribution of oxidation by O_2 (estimated using the Nagle and Strickland-Constable [10] correlation). First of all, it is evident that allowing for direct oxidation by O_2 generally has a small effect on the collision efficiencies estimated in Fig. 12. In addition, there is significant scatter (more than a factor of 10) of the present collision efficiencies for diffusion flames and even larger scatter (nearly a factor of 100) of the collision efficiencies of Neoh et al. [21] in premixed flames. These findings clearly do not support CO_2 as a major direct contributor to soot oxidation in flames either alone or in parallel with soot oxidation by O_2.

The collision efficiencies of H_2O for soot oxidation are plotted as a function of height above the burner in Fig. 13, in the same manner as the results for CO_2 oxidation of soot in Fig. 12. The observations are the same: O_2 oxidation makes only a minor contribution to soot

oxidation in parallel with H_2O and H_2O collision efficiencies exhibit large scatter (nearly a factor of 100) in both premixed and diffusion flames. These findings also clearly do not support H_2O as a major direct contributor to soot oxidation in flames either alone or in parallel with soot oxidation by O_2.

The collision efficiencies of O for soot oxidation are plotted as a function of height above the burner in Fig. 14, in the same manner as the results for CO_2 and H_2O oxidation of soot in Figs. 12 and 13. The results are much the same: direct O_2 oxidation is not very important and collision efficiencies of O exhibit large scatter (more than a factor of 10) in both premixed and diffusion flames. In addition, relatively small concentrations of O compared to other potential oxidizing aspecies in both the premixed and diffusion flames would require unrealistic collision efficiencies greater than unity if O was the major soot oxidizing species for the results illustrated in Fig. 14. These findings clearly also do not support O as a major direct contributor to soot oxidation in flame environments.

Finally, the collision efficiencies of OH for soot oxidation are plotted as a function of height above the burner in Fig. 15, in the same manner as the results for CO_2 and H_2O and O oxidation of soot in Figs. 11-14. With perhaps one exception, direct O_2 oxidation of soot is not very important for these conditions, as before. On the other hand, similar to the observations of Neoh et al. [21], present collision efficiencies of OH exhibit relatively small levels of scatter (roughly a factor of 3). Furthermore, the results for premixed and diffusion flames in Fig. 15 exhibit remarkably good agreement with each other. In particular, the collision efficiency of OH for soot oxidation in the present diffusion flames is 0.10 with a standard deviation of 0.07; this is in excellent agreement with the value for soot oxidation from Neoh et al. [21] in premixed flames of 0.13 when using the same treatment of soot structure. Finally, this agreement was achieved over a relatively broad range of flame conditions for the combined results in premixed

and diffusion flames, as follows: temperatures of 1570-1870 K, oxygen mole fractions of 1×10^{-5} – 1.2×10^{-2} and levels of soot mass consumption less than 70% at atmospheric pressure. While these results are helpful, however, the properties of the final stage of oxidation, where internal oxidation of primary particles becomes a factor, effects of pressure on soot oxidation, and possibly effects of fuel type on soot oxidation for hydrocarbons other than those considered here, all merit additional study in the future.

CONCLUSIONS

Flame structure and soot oxidation processes were studied in the soot oxidation region of coflowing laminar jet diffusion flames. Test conditions involved acetylene-nitrogen, ethylene-, propylene-nitrogen and propane fuel mixtures burning in air at atmospheric pressure as summarized in Table 1. For these flames, O_2 mole fractions were generally smaller than 5% in the region where soot oxidation was observed. The major conclusions of the study are as follows:

1. Potential soot oxidizing species in the region that was studied include O_2, CO_2, H_2O, O and OH with OH and H exhibiting superequilibrium concentrations by factors as large as 10-20. The radical O exhibited even larger superequilibrium ratios, up to 1000, but absolute concentrations of O were generally significantly smaller than concentrations of OH and H. Among these species, OH was mainly responsible for soot oxidation with significant levels of soot oxidation beginning at fuel-rich conditions and proceeding in parallel with soot formation in the region where acetylene was still present.

2. Soot oxidation rates could be correlated by assuming a constant collision efficiency of OH for soot of 0.10 with a standard deviation of 0.07, with no significant effect of fuel type observed for this behavior. This finding is in good agreement with the OH collision

efficiency of soot of 0.13 for assumed similar soot structure properties found by Neoh et al. [21] for measurements in premixed flames at similar O_2 concentrations and atmospheric pressure. Earlier observations of large variations of OH collision efficiencies for soot in diffusion flames due to Garo et al. [27,28], Puri et al. [29,30] and Haudiquert et al. [31] probably were caused by the use of optical methods to find soot structure that have not proven to be effective for soot aggregates, see Wersborg et al. [32] and Köylü and Faeth [33].

3. The correction of present soot oxidation rates for oxidation by O_2 based on the results of Nagle and Strickland-Constable [10] was small (on average less than 10%) compared to oxidation by OH for present conditions. Soot oxidation at leaner conditions, particularly when temperatures are elevated, should exhibit a larger contribution from O_2; this transition has received little attention, however, and merits additional study in the future. Other issues concerning soot oxidation that merit attention in the future include effects of internal oxidation in the final stages of oxidation, effects of pressure, and additional study of effects of fuel type.

This research was sponsored by NASA grants NCC3-661, NAG-3-1878, NAG-3-2048 and NAG3-2404 under the technical management of D. L. Urban and Z.-G. Yuan of the NASA Glenn Research Center.

REFERENCES

1. Sunderland, P.B., Köylü, Ü.Ö., and Faeth, G.M., Combust. Flame 100:310 (1995).

2. Sunderland, P.B., and Faeth, G.M., Combust. Flame 105:132 (1996).

3. Lin, K.-C., Sunderland, P.B., and Faeth, G.M., Combust. Flame 104:375 (1996).

4. Xu, F., Sunderland, P.B., and Faeth, G.M., Combust. Flame 108:471 (1997).

5. Xu, F., Lin, K.-C., and Faeth, G.M., Combust. Flame 115:195 (1998).

6. Xu, F., and Faeth, G.M., Combust. Flame 121:640 (2000).

7. Xu, F., and Faeth, G.M., Combust. Flame, in press.

8. Xu, F., *Soot Growth in Laminar Premixed Flames*, Ph.D. Thesis, The University of Michigan, 1999.

9. Xu, F., El-Leathy, A.M., Sunderland, P.B., Dai, Z., and Faeth, G.M., *Laminar Soot Processes (LSP)*, Report No. GDL-GMF-00-03, Department of Aerospace Engineering, The University of Michigan, Ann Arbor, MI, 2000.

10. Nagle, J., and Strickland-Constable, R.F., *Proceedings of Fifth Carbon Conference* 1:154 (1962).

11. Rosner, D.E., and Allendorf, H.D., AIAA J. 6:650 (1968).

12. Wright, F.J., Proc. Combust. Inst. 15:1449 (1974).

13. Radcliffe, S.W., and Appleton, J.P., Combust. Sci. Tech. 4:171 (1971).

14. Park, C., and Appleton, J.P., Combust. Flame 20:369 (1973).

15. Libby, P.A., and Blake, T.R., Combust. Flame 36:139 (1979).

16. Libby, P.A., and Blake, T.R., Combust. Flame 41:123 (1981).

17. Johnstone, J.F., Chen, C.Y., and Scott, D.S., Ind. Engr. Chem. 44:1564 (1952).

18. Bradley, D., Dixon-Lewis, G., El-Din Habik, S., and Mushi, E.M.J., Proc. Combust. Inst. 20:931 (1984).

19. Fenimore, C.P., and Jones, C.W., J. Phys. Chem. 71:593 (1967).

20. Mulcahy, M.F.R., and Young, B.C., Carbon 13:115 (1975).

21. Neoh, K.G., Howard, J.B., and Sarofim, A.F., *Particulate Carbon* (D.C. Siegla and B.W. Smith, ed.), Plenum Press, New York, 1980, p. 261.

22. Neoh, K.G., *Soot Burnout in Flames*, Ph.D. Thesis, Massachusetts Institute of Technology, Cambridge, MA, 1980.

23. Neoh, K.G., Howard, J.B., and Sarofim, A.F., Proc. Combust. Inst. 20:951 (1984).

24. Wicke, B.C., Wong, C., and Grady, K.A., Combust. Flame 66:37 (1986).

25. Wicke, B.C., and Grady, K.A., Combust. Flame 69:185 (1987).

26. Roth, P., Brandt, O., and von Gersum, S., Proc. Combust. Inst. 23:1485 (1990).

27. Garo, A., Lahaye, J., and Prado, G., Proc.Combust. Inst. 21:1023 (1986).

28. Garo, A., Prado, G., and Lahaye, J., Combust. Flame Vol. 79:226 (1990).

29. Puri, R., Santoro, R.J., and Smyth, K.C., Combust. Flame 97:125 (1994).

30. Puri, R., Santoro, R.J., and Smyth, K.C., Combust. Flame 102:226 (1995).

31. Haudiquert, M., Cessou, A., Stepowki, D., and Coppalle, A., Combust. Flame 111:338 (1997).

32. Wersborg, B.L., Howard, J.B., and Williams, G.C., Proc. Combust. Inst. 14:929 (1972).

33. Köylü, Ü.Ö., and Faeth, G.M., J. Heat Trans. 115:409 (1993).

34. Dalzell, W.H., and Sarofim, A.F., J. Heat Trans. 91:100 (1969).

35. Krishnan, S.S., Lin, K.-C., and Faeth, G.M., J. Heat Trans. 122:517 (2000).

36. Chase, M.W., Jr. Davies, C.A., Downey, J.R., Jr., Frurip, D.J., McDonald, R.R., and Syverud, A.N., *JANAF Thermochemical Tables*, 3rd ed., J. Phys. Chem. Ref. Data 14 (Supplement 1): 1211 (1986).

37. McBride, B.J., Reno, M.A., and Gordon, S., *CET93 and CETPC: An Interim Updated Version of the NASA Lewis Computer Program for Calculating Complex Chemical Equilibrium with Applications.* NASA Technical Memorandum 4557, Washington, D.C., 1994.

38. Hamins, A., Gordon, A.S., Saito, K., and Seshadri, K., Combust. Sci. Tech. 45:309 (1986).

39. Colket, M.B, III, Seery, D.J., and Palmer, H.B., Combust. Flame 75:343 (1989).

40. Colket, M.B, III, Seery, D.J., and Palmer, H.B., Combust. Flame 84:434 (1991).

41. Tesner, P.A., Proc. Combust. Inst. 7:536 (1958).

42. Tesner, P.A., Proc. Combust. Inst. 8:627 (1960).

43. Colket, M.B., and Hall, R.J., in *Soot Formation in Combustion* (H. Bockhorn, ed.), Springer-Verlag, Berlin, 1994, p. 442.

Table 1 Summary of the test laminar jet diffusion flames[a]

Flame	1	2	3	4	5	6
Fuel	C_2H_2	C_2H_2	C_2H_2	C_2H_4	C_3H_6	C_3H_8
Burner flow (% fuel by volume in N_2)	16.9	15.1	17.1	100.0	18.8	100.0
Burner exit velocity (mm/s)	27.4	31.4	32.4	5.8	17.4	3.4
Air coflow velocity (mm/s)	55.5	55.5	55.5	171	130	130
Luminous flame length (mm)	82	80	103	100	100	100
Stoichiometric flame length (mm)	100	106	116	81	74	79
Re (-)[b]	62	71	74	23	92	25
$Fr \times 10^5$ (-)[b]	220.0	290.0	310.0	9.9	89.0	3.3
Stoichiometric flame temperature (K)	2380	2320	2390	2366	2147	2263

[a]Laminar round jet diffusion flames with a 34.8 mm inside diameter fuel port and a 60 mm inside diameter concentric outer port flowing air. Ambient temperature and pressure of 294 ± 2 K and 98 ± 1 kPa, respectively. Gas purities (by volume): nitrogen, 99.9%; oxygen, 99.6%; acetylene, 99.6%; ethylene, 99.5%; propylene, 99.5%; propane, 99.5%; laboratory air coflow having a 240 K dewpoint.

[b]Normal value based on mean burner exit velocity.

List of Figures

Fig. 1 Dark-field photograph of a typical laminar jet diffusion flame: the ethylene-fueled flame burning in air at atmospheric pressure.

Fig. 2 Typical TEM photographs of soot aggregates along the axis of the ethylene-fueled laminar jet diffusion flame burning in air at atmospheric pressure: left photograph near start of soot formation (z = 20 mm), center photograph near the maximum soot concentration condition (z = 50 mm), right photograph near the end of soot oxidization (z = 70 mm).

Fig. 3 Measured soot and flame properties along the axis of an acetylene-nitrogen/air laminar jet diffusion flame at roughly atmospheric pressure (Flame 1, fuel stream of 16.9% C_2H_2 and 83.1% N_2 by volume).

Fig. 4 Measured soot and flame properties along the axis of an ethylene/air air laminar jet diffusion flame at roughly atmospheric pressure (Flame 4).

Fig. 5 Measured soot and flame properties along the axis of a propylene-nitrogen/air laminar jet diffusion flame at roughly atmospheric pressure (Flame 5, fuel stream of 18.8% C_3H_6 and 81.2% N_2 by volume).

Fig. 6 Measured soot and flame properties along the axis of a propane/air laminar jet diffusion flame at roughly atmospheric pressure (Flame 6).

Fig. 7 Fuel-equivalence ratios and superequilibrium ratios of H, OH and O along the axis of the acetylene/air laminar jet diffusion flames at roughly atmospheric pressure.

Fig. 8 Fuel-equivalence ratios and superequilibrium ratios of H, OH and O along the axis of ethylene, propylene and propane/air laminar jet diffusion flames at roughly atmospheric pressure.

Fig. 9 Derived soot oxidation properties (S, n_p and w_{ox}) along the axes of acetylene/air laminar jet diffusion flames at roughly atmospheric pressure.

Fig. 10 Derived soot oxidation properties (S, n_p and w_{ox}) along the axes of the ethylene, propylene, and propane/air laminar jet diffusion flames at roughly atmospheric pressure.

Fig. 11 Collision efficiencies assuming soot burnout due to attack by O_2 as a function of height above the burner. Found from the measurements of Neoh et al. [21] in premixed flames, estimated from the predictions of Nagle and Strickland-Constable [10] for the conditions of the present diffusion flames, and found from present measurements in diffusion flames.

Fig. 12 Collision efficiencies assuming soot burnout due to attack by CO_2 as a function of height above the burner. Found from the measurements of Neoh et al. [21] in premixed flames, and from the present measurements in diffusion flames with and without parallel O_2 attack estimated from the predictions of Nagle and Strickland-Constable [10].

Fig. 13 Collision efficiencies assuming soot burnout due to attack by H_2O as a function of height above the burner. Found from the measurements of Neoh et al. [21] in premixed flames, and from the present measurements in diffusion flames with and without parallel O_2 attack estimated from the predictions of Nagle and Strickland-Constable [10].

Fig. 14 Collision efficiencies assuming soot burnout due to attack by O as a function of height above the burner. Found from the measurements of Neoh et al. [21] in premixed flames, and from the present measurements in diffusion flames with and without parallel O_2 attack estimated from the predictions of Nagle and Strickland-Constable [10].

Fig. 15 Collision efficiencies assuming soot burnout due to attack by OH as a function of height above the burner. Found from the measurements of Neoh et al. [21] in premixed flames, and from the present measurements in diffusion flames with and without parallel O_2 attack estimated from the predictions of Nagle and Strickland-Constable [10].

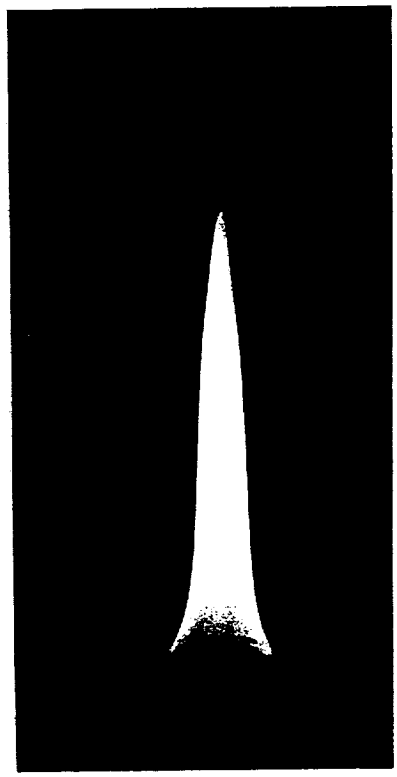

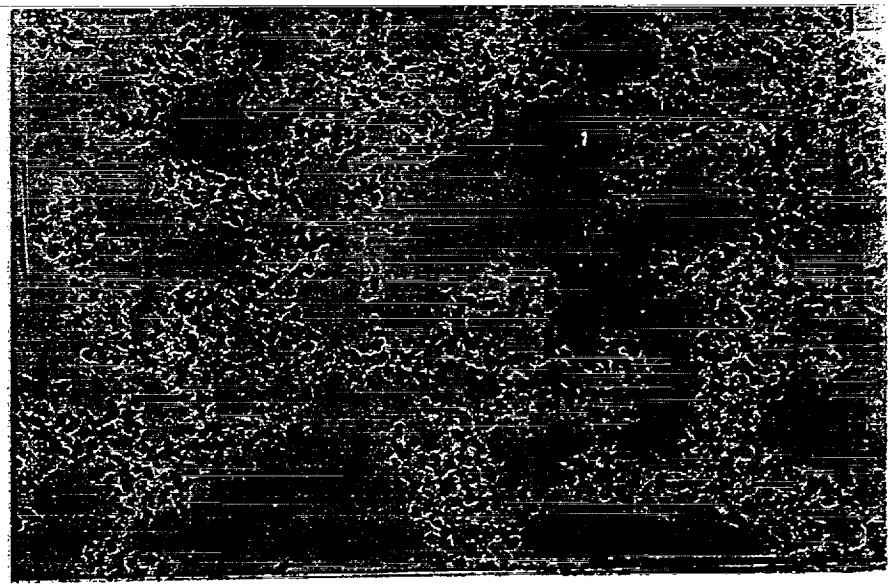

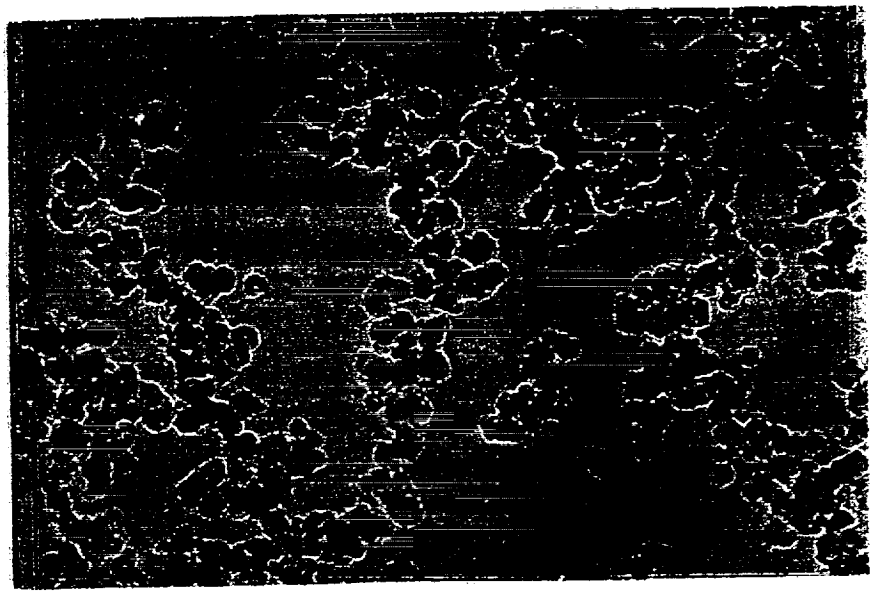

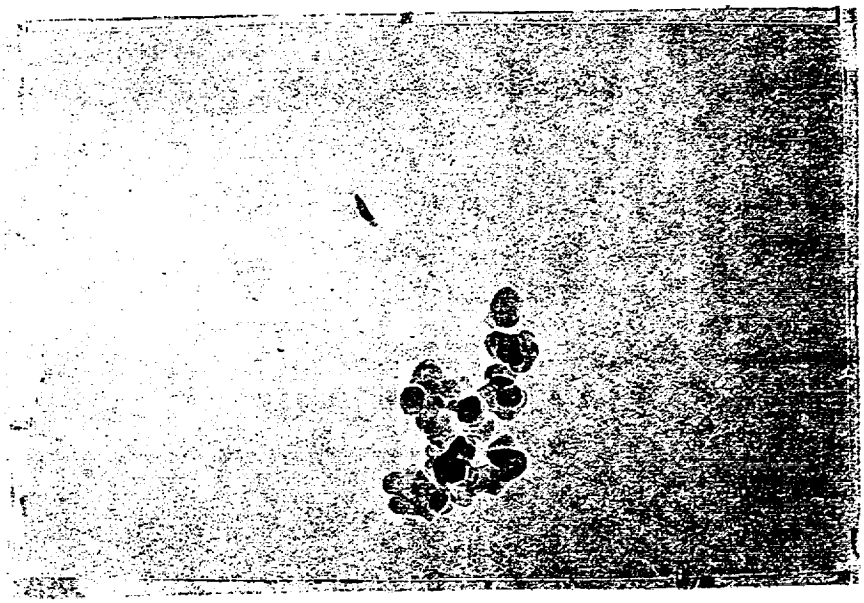

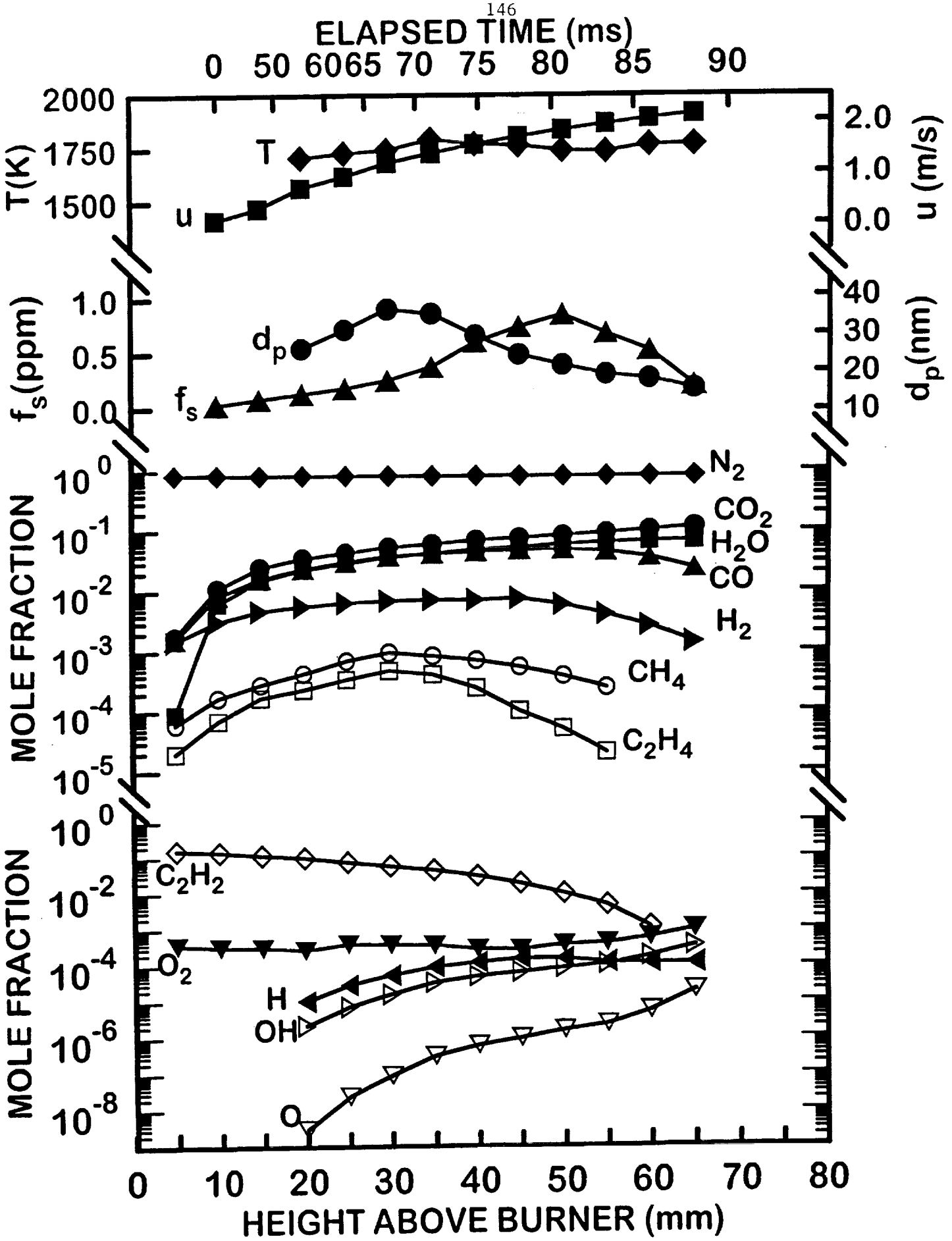
ELAPSED TIME (ms)
0 50 6065 70 75 80 85 90
T(K)
2000
1750
1500
T
u
u (m/s)
2.0
1.0
0.0
f_s(ppm)
1.0
0.5
0.0
d_p
f_s
d_p(nm)
40
30
20
10
MOLE FRACTION
10^0
10^{-1}
10^{-2}
10^{-3}
10^{-4}
10^{-5}
N_2
CO_2
H_2O
CO
H_2
CH_4
C_2H_4
MOLE FRACTION
10^0
10^{-2}
10^{-4}
10^{-6}
10^{-8}
C_2H_2
O_2
H
OH
O
0 10 20 30 40 50 60 70 80
HEIGHT ABOVE BURNER (mm)

(3)

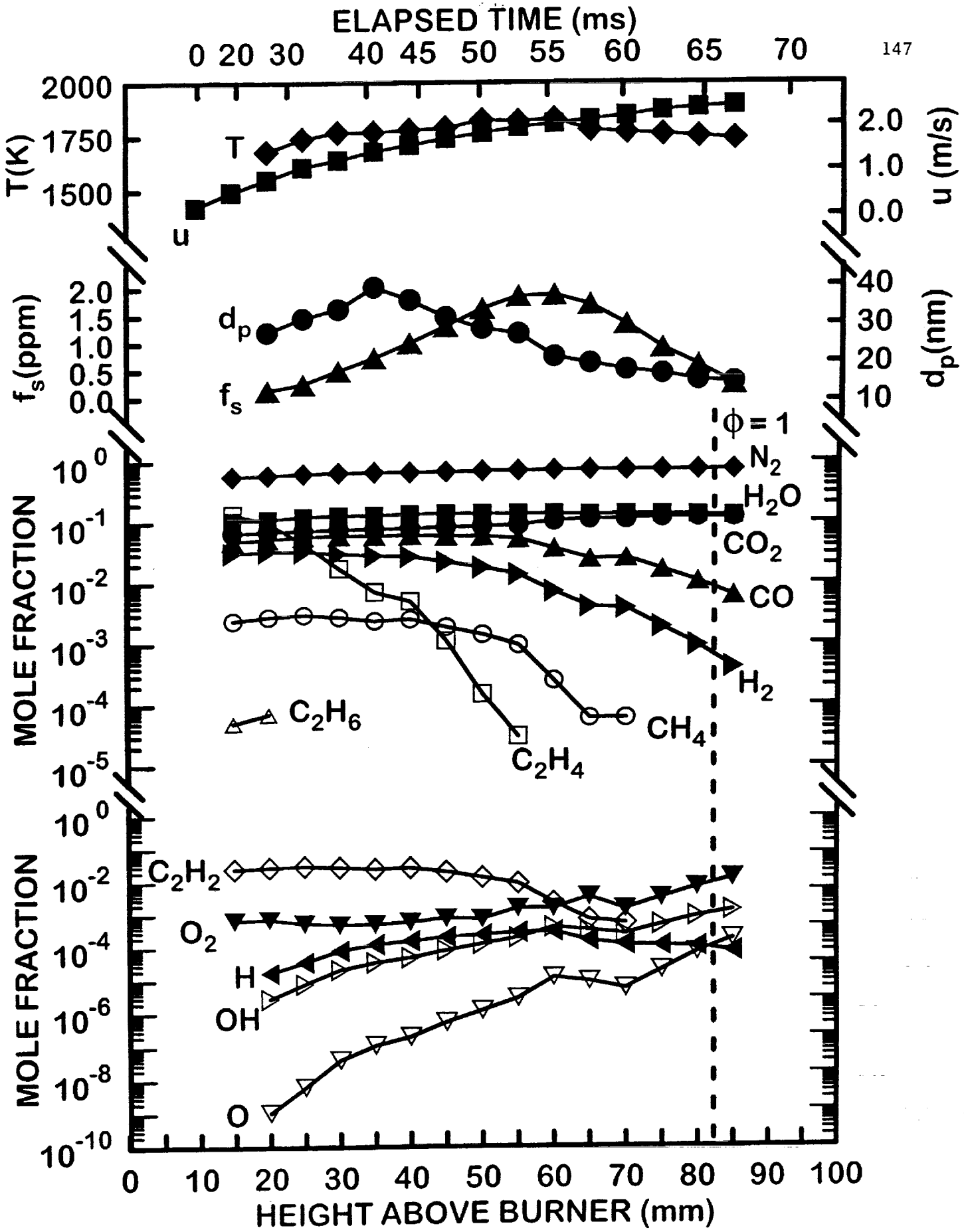
ELAPSED TIME (ms)
0 20 30 40 45 50 55 60 65 70
T(K)
2000
1750
1500
T
u
u (m/s)
2.0
1.0
0.0
f_s(ppm)
2.0
1.5
1.0
0.5
0.0
d_p
f_s
d_p(nm)
40
30
20
10
MOLE FRACTION
10^0
10^{-1}
10^{-2}
10^{-3}
10^{-4}
10^{-5}
$\phi = 1$
N_2
H_2O
CO_2
CO
H_2
C_2H_6
CH_4
C_2H_4
MOLE FRACTION
10^0
10^{-2}
10^{-4}
10^{-6}
10^{-8}
10^{-10}
C_2H_2
O_2
H
OH
O
0 10 20 30 40 50 60 70 80 90 100
HEIGHT ABOVE BURNER (mm)

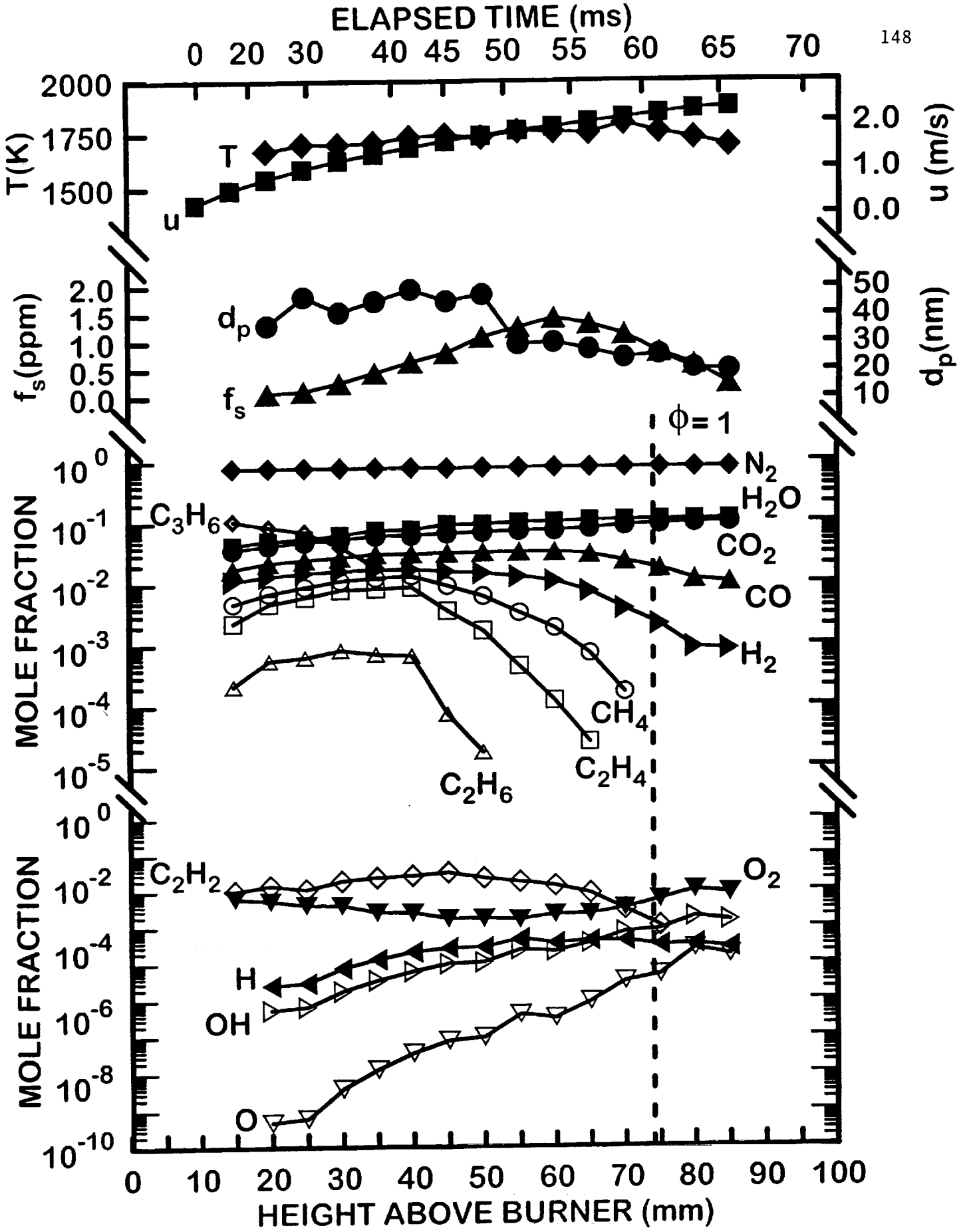
ELAPSED TIME (ms)
0 20 30 40 45 50 55 60 65 70
T(K)
2000
1750
1500
T
u
u (m/s)
2.0
1.0
0.0
f_s(ppm)
2.0
1.5
1.0
0.5
0.0
d_p
f_s
d_p(nm)
50
40
30
20
10
ϕ= 1
MOLE FRACTION
10^0
10^{-1}
10^{-2}
10^{-3}
10^{-4}
10^{-5}
N_2
H_2O
C_3H_6
CO_2
CO
H_2
CH_4
C_2H_4
C_2H_6
MOLE FRACTION
10^0
10^{-2}
10^{-4}
10^{-6}
10^{-8}
10^{-10}
C_2H_2
O_2
H
OH
O
0 10 20 30 40 50 60 70 80 90 100
HEIGHT ABOVE BURNER (mm)

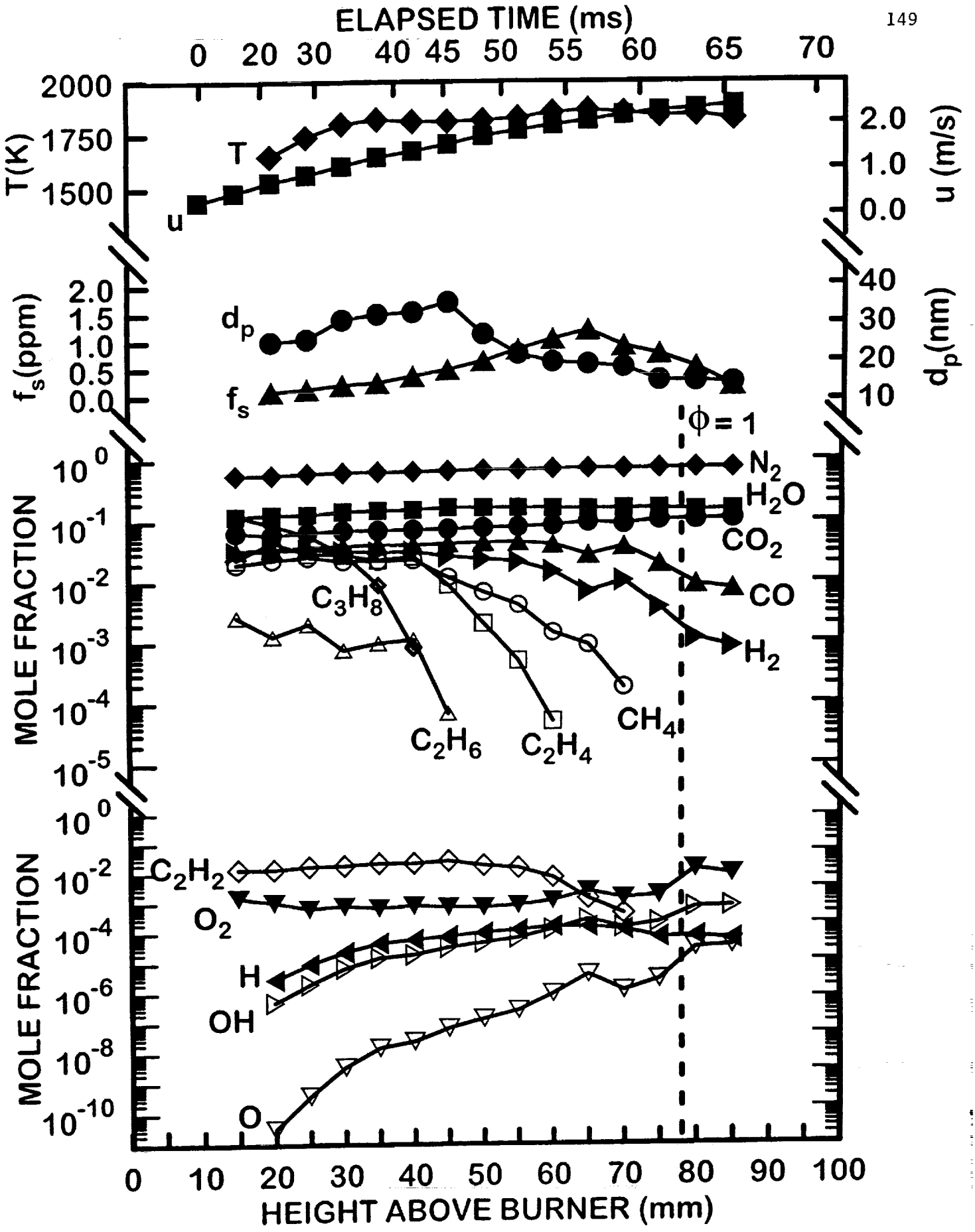
ELAPSED TIME (ms)
0 20 30 40 45 50 55 60 65 70
T(K)
2000
1750
1500
T
u
2.0
1.0
0.0
u (m/s)
f_s(ppm)
2.0
1.5
1.0
0.5
0.0
d_p
f_s
40
30
20
10
d_p(nm)
$\phi = 1$
MOLE FRACTION
10^0
10^{-1}
10^{-2}
10^{-3}
10^{-4}
10^{-5}
N_2
H_2O
CO_2
CO
H_2
C_3H_8
C_2H_6
C_2H_4
CH_4
MOLE FRACTION
10^0
10^{-2}
10^{-4}
10^{-6}
10^{-8}
10^{-10}
C_2H_2
O_2
H
OH
O
0 10 20 30 40 50 60 70 80 90 100
HEIGHT ABOVE BURNER (mm)

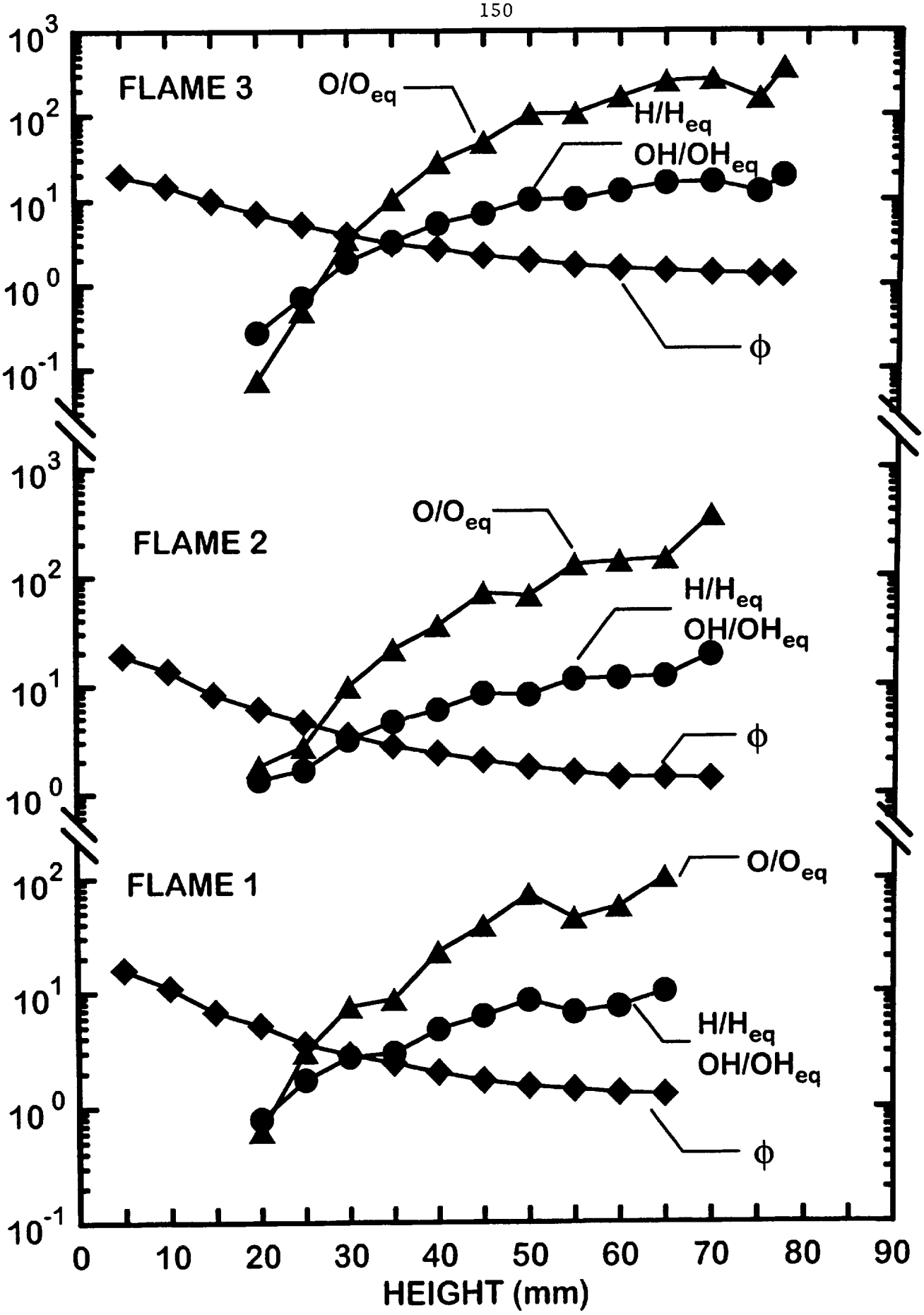
FLAME 3
O/O$_{eq}$
H/H$_{eq}$
OH/OH$_{eq}$
ϕ
FLAME 2
O/O$_{eq}$
H/H$_{eq}$
OH/OH$_{eq}$
ϕ
FLAME 1
O/O$_{eq}$
H/H$_{eq}$
OH/OH$_{eq}$
ϕ
10^3
10^2
10^1
10^0
10^{-1}
0
10
20
30
40
50
60
70
80
90
HEIGHT (mm)

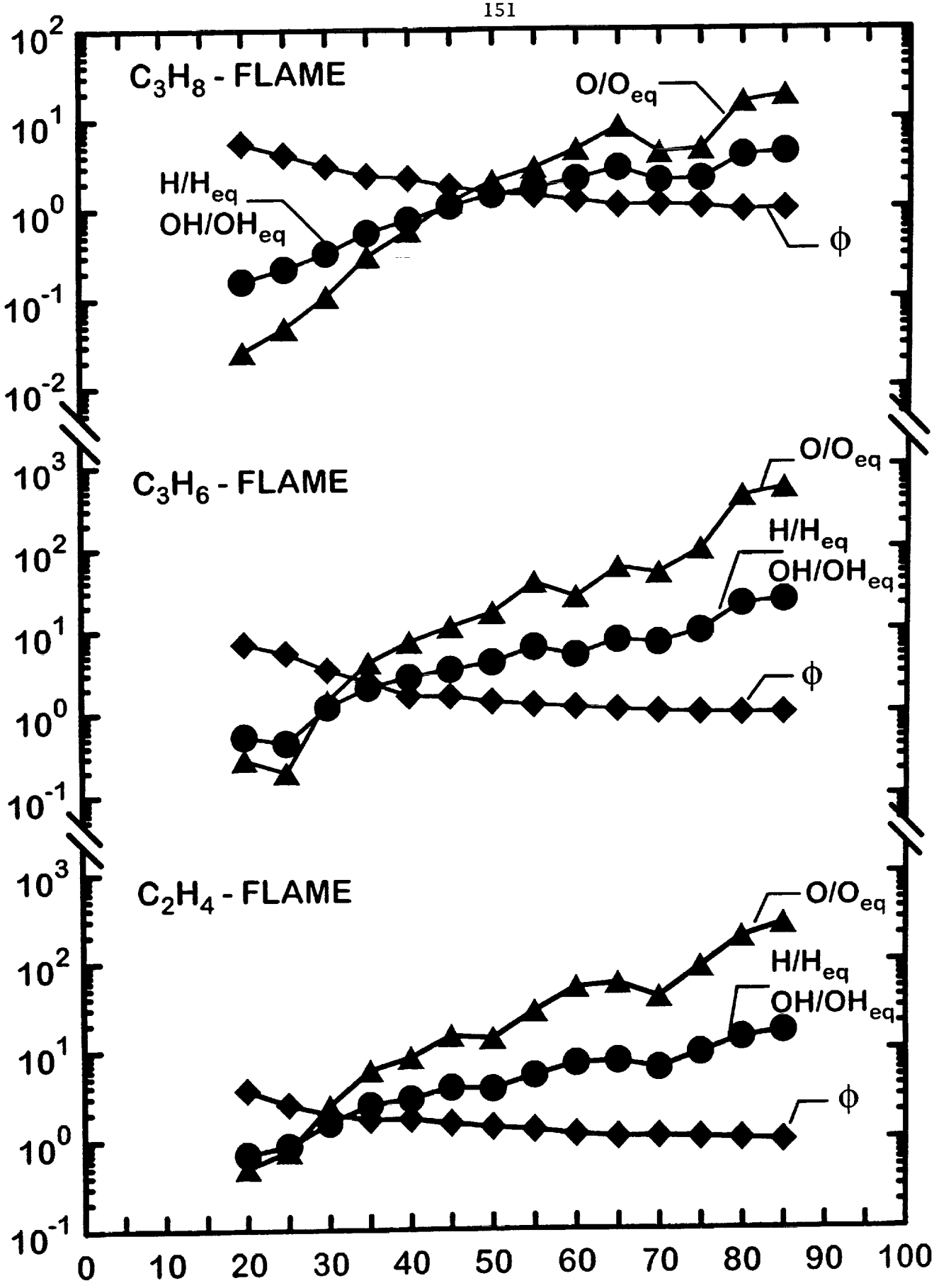
C_3H_8 - FLAME
O/O_{eq}
H/H_{eq}
OH/OH_{eq}
ϕ
C_3H_6 - FLAME
O/O_{eq}
H/H_{eq}
OH/OH_{eq}
ϕ
C_2H_4 - FLAME
O/O_{eq}
H/H_{eq}
OH/OH_{eq}
ϕ
10^2
10^1
10^0
10^{-1}
10^{-2}
10^3
10^2
10^1
10^0
10^{-1}
10^3
10^2
10^1
10^0
10^{-1}
0
10
20
30
40
50
60
70
80
90
100

(8)

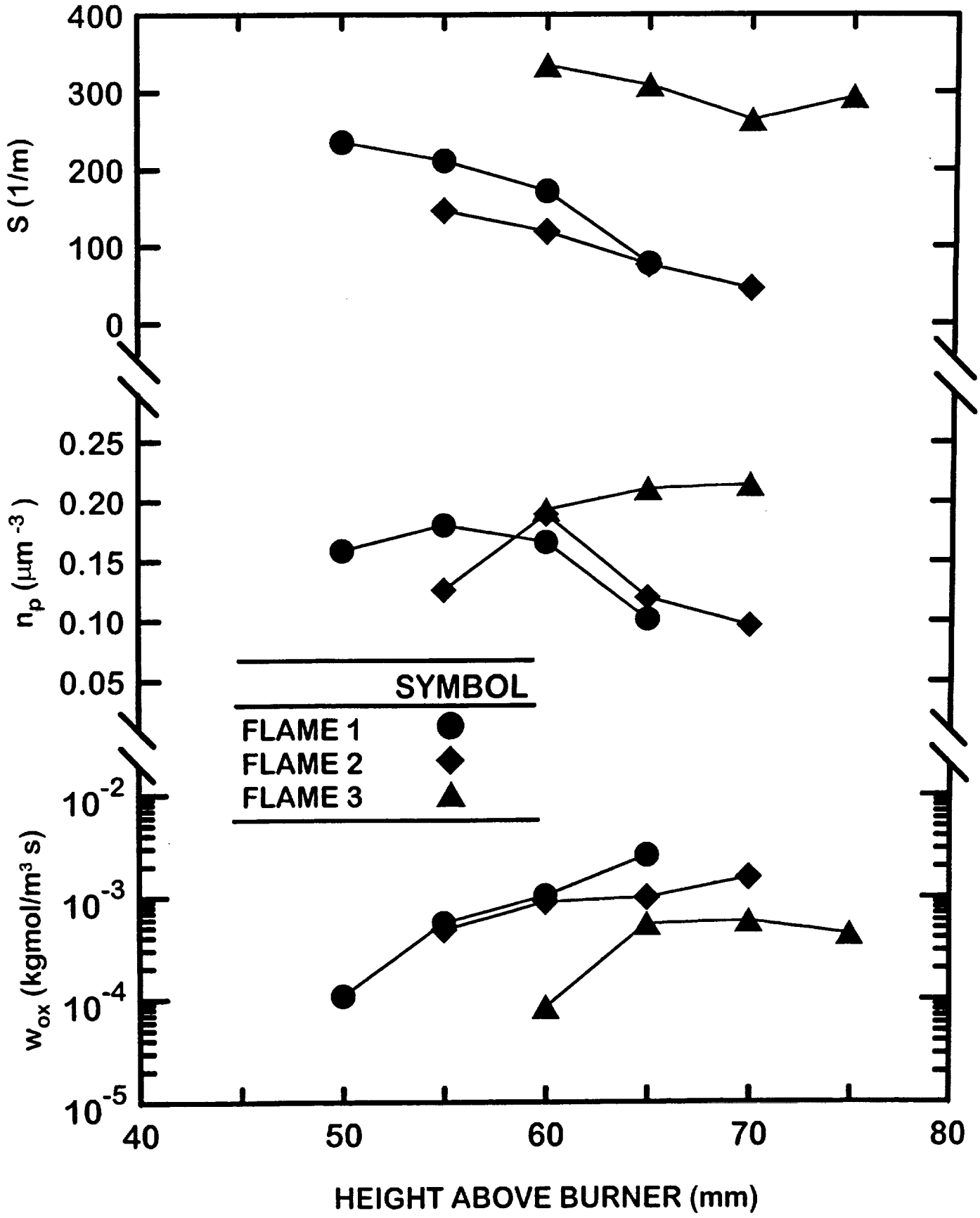
400
300
200
100
0
S (1/m)
0.25
0.20
0.15
0.10
0.05
n_p (μm^{-3})
SYMBOL
FLAME 1
FLAME 2
FLAME 3
10^{-2}
10^{-3}
10^{-4}
10^{-5}
w_{ox} (kgmol/m^3 s)
40
50
60
70
80
HEIGHT ABOVE BURNER (mm)

(9)

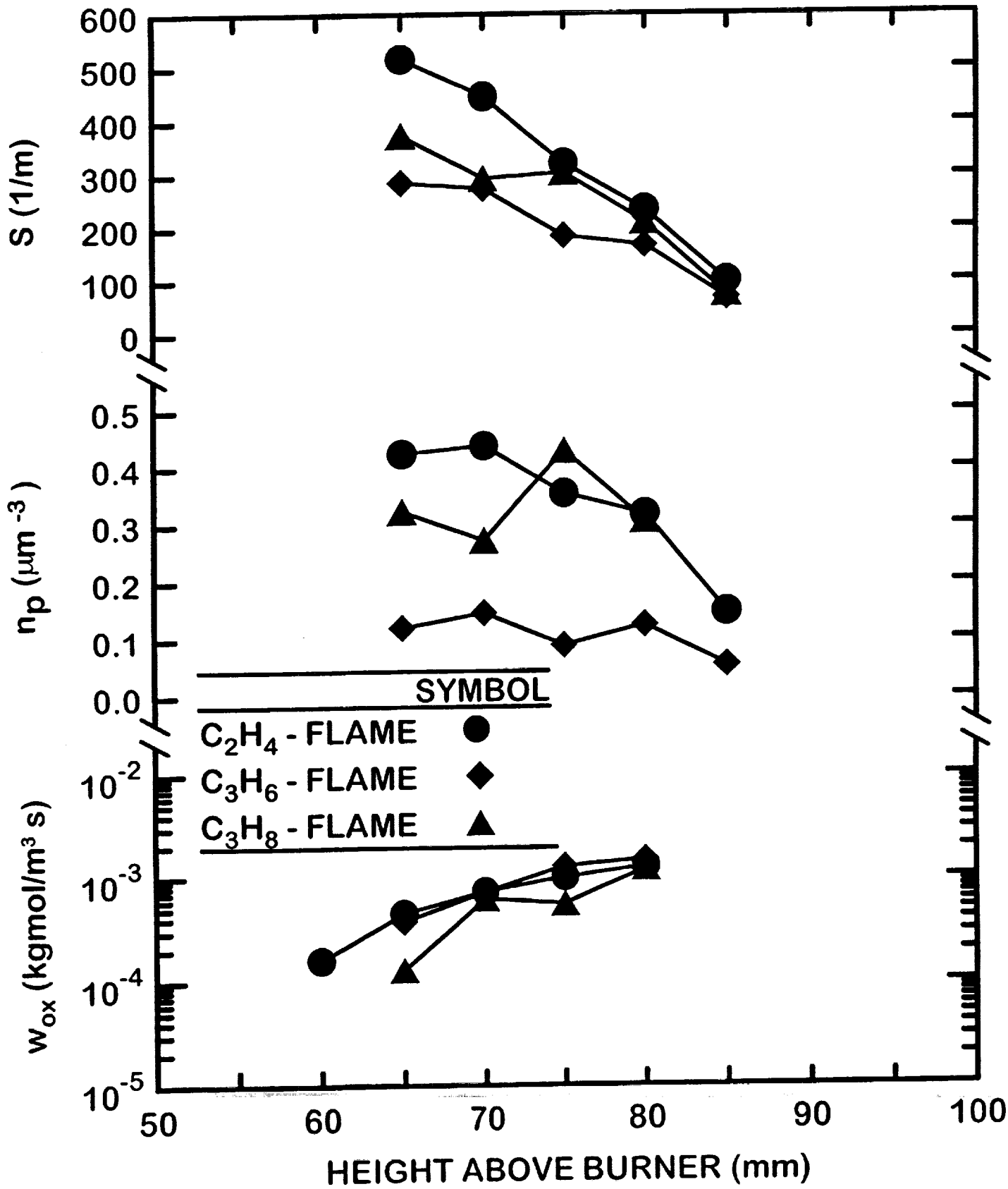
S (1/m)
600
500
400
300
200
100
0
n_p (μm^{-3})
0.5
0.4
0.3
0.2
0.1
0.0
w_{ox} (kgmol/m³ s)
10^{-2}
10^{-3}
10^{-4}
10^{-5}
SYMBOL
C_2H_4 - FLAME
C_3H_6 - FLAME
C_3H_8 - FLAME
50
60
70
80
90
100
HEIGHT ABOVE BURNER (mm)

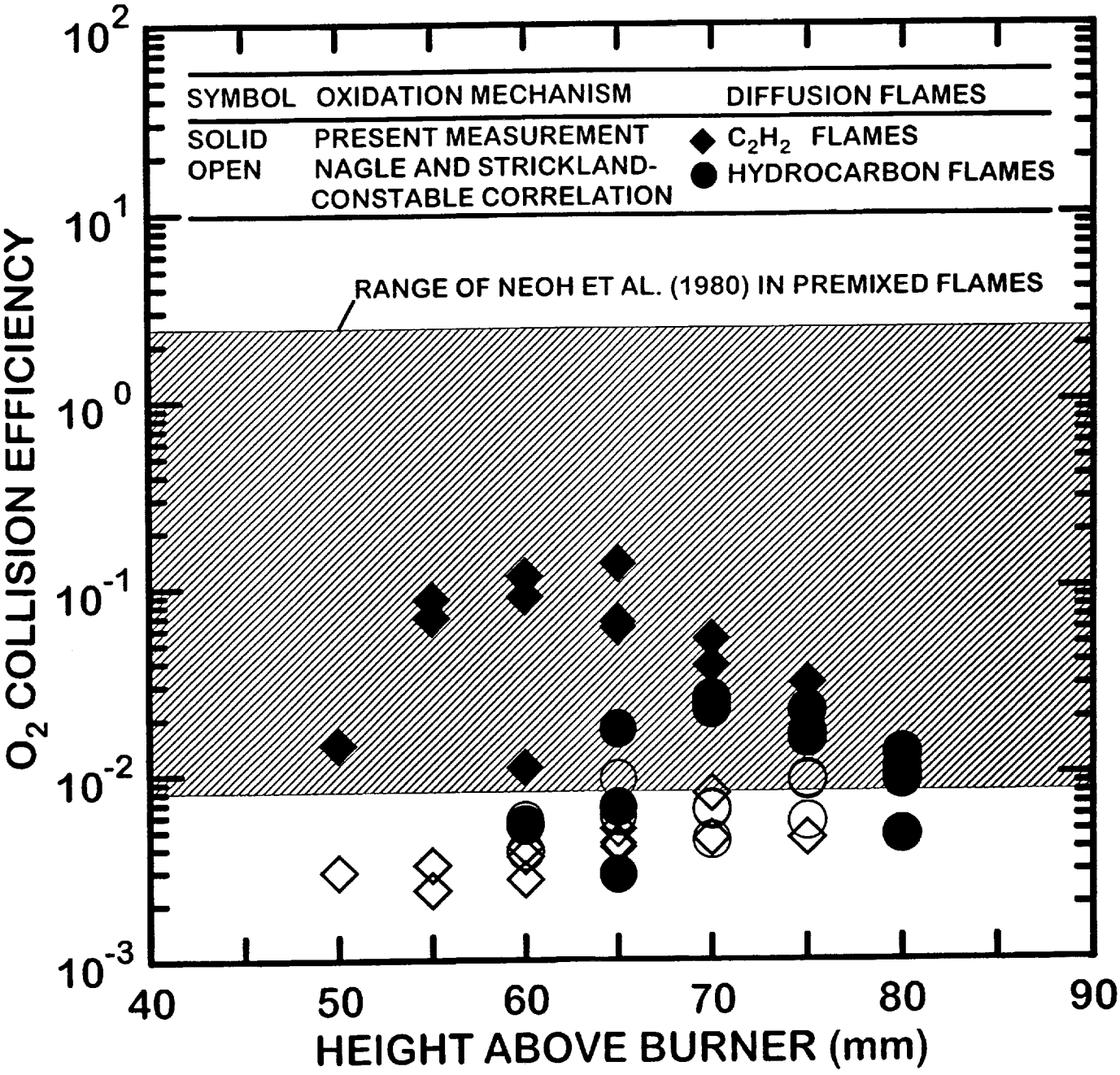
SYMBOL OXIDATION MECHANISM DIFFUSION FLAMES
SOLID PRESENT MEASUREMENT C_2H_2 FLAMES
OPEN NAGLE AND STRICKLAND-CONSTABLE CORRELATION HYDROCARBON FLAMES
RANGE OF NEOH ET AL. (1980) IN PREMIXED FLAMES
O_2 COLLISION EFFICIENCY
10^2
10^1
10^0
10^{-1}
10^{-2}
10^{-3}
40
50
60
70
80
90
HEIGHT ABOVE BURNER (mm)

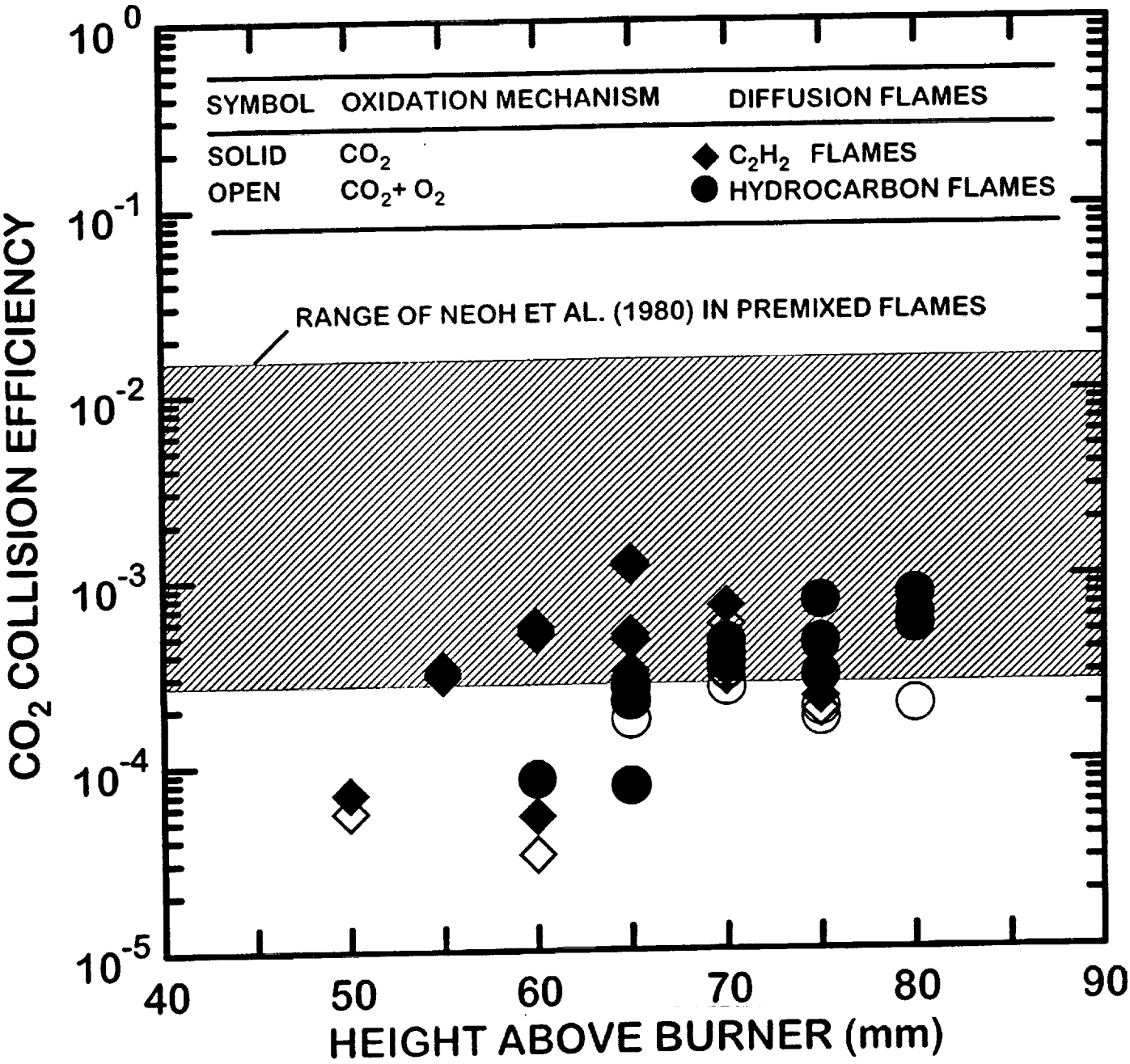
SYMBOL OXIDATION MECHANISM DIFFUSION FLAMES
SOLID CO_2
OPEN $CO_2 + O_2$
C_2H_2 FLAMES
HYDROCARBON FLAMES
RANGE OF NEOH ET AL. (1980) IN PREMIXED FLAMES
CO_2 COLLISION EFFICIENCY
10^0
10^{-1}
10^{-2}
10^{-3}
10^{-4}
10^{-5}
40
50
60
70
80
90
HEIGHT ABOVE BURNER (mm)

(17)

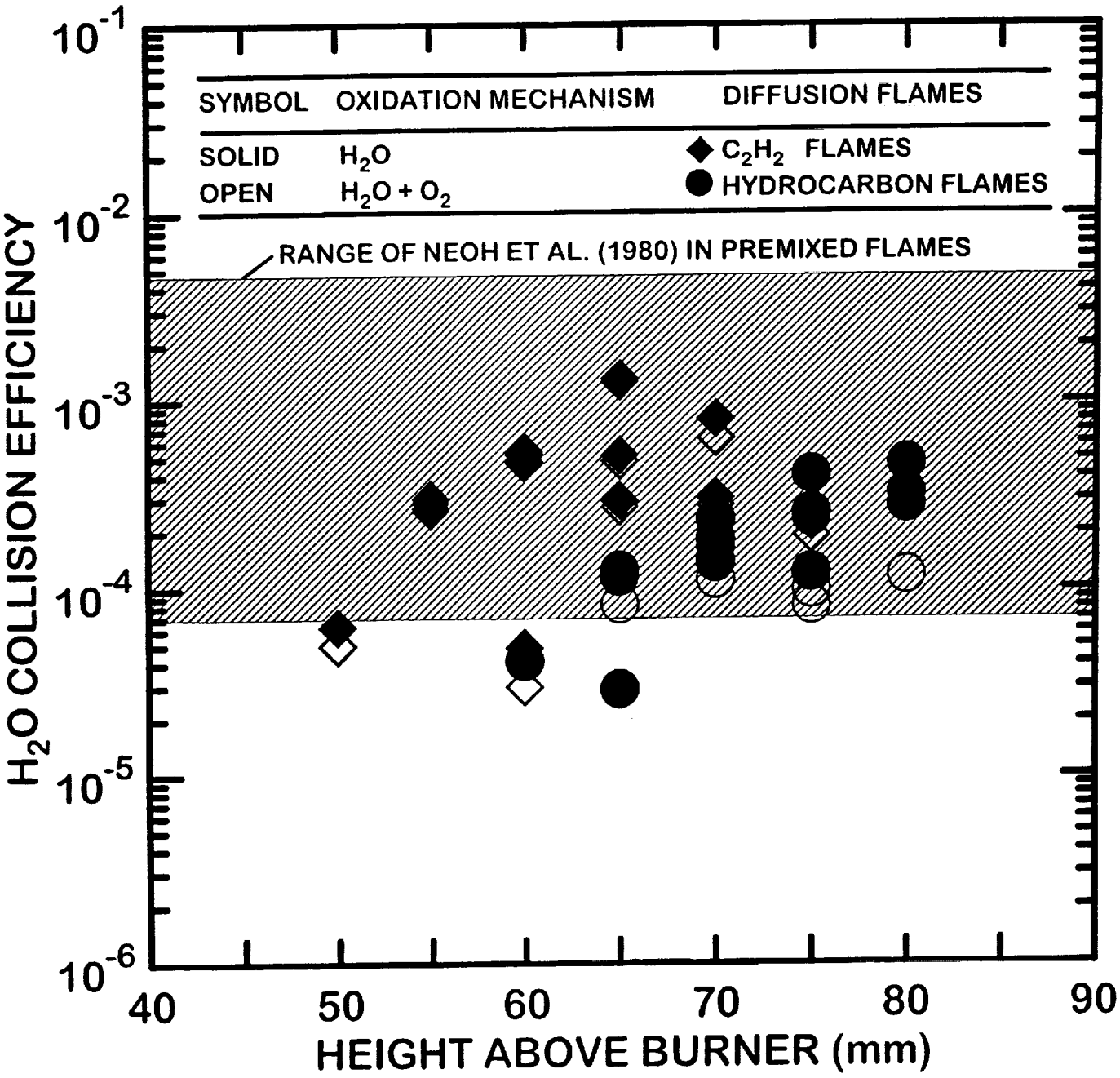
SYMBOL OXIDATION MECHANISM DIFFUSION FLAMES
SOLID H_2O
OPEN $H_2O + O_2$
C_2H_2 FLAMES
HYDROCARBON FLAMES
RANGE OF NEOH ET AL. (1980) IN PREMIXED FLAMES
H_2O COLLISION EFFICIENCY
10^{-1}
10^{-2}
10^{-3}
10^{-4}
10^{-5}
10^{-6}
40
50
60
70
80
90
HEIGHT ABOVE BURNER (mm)

(13)

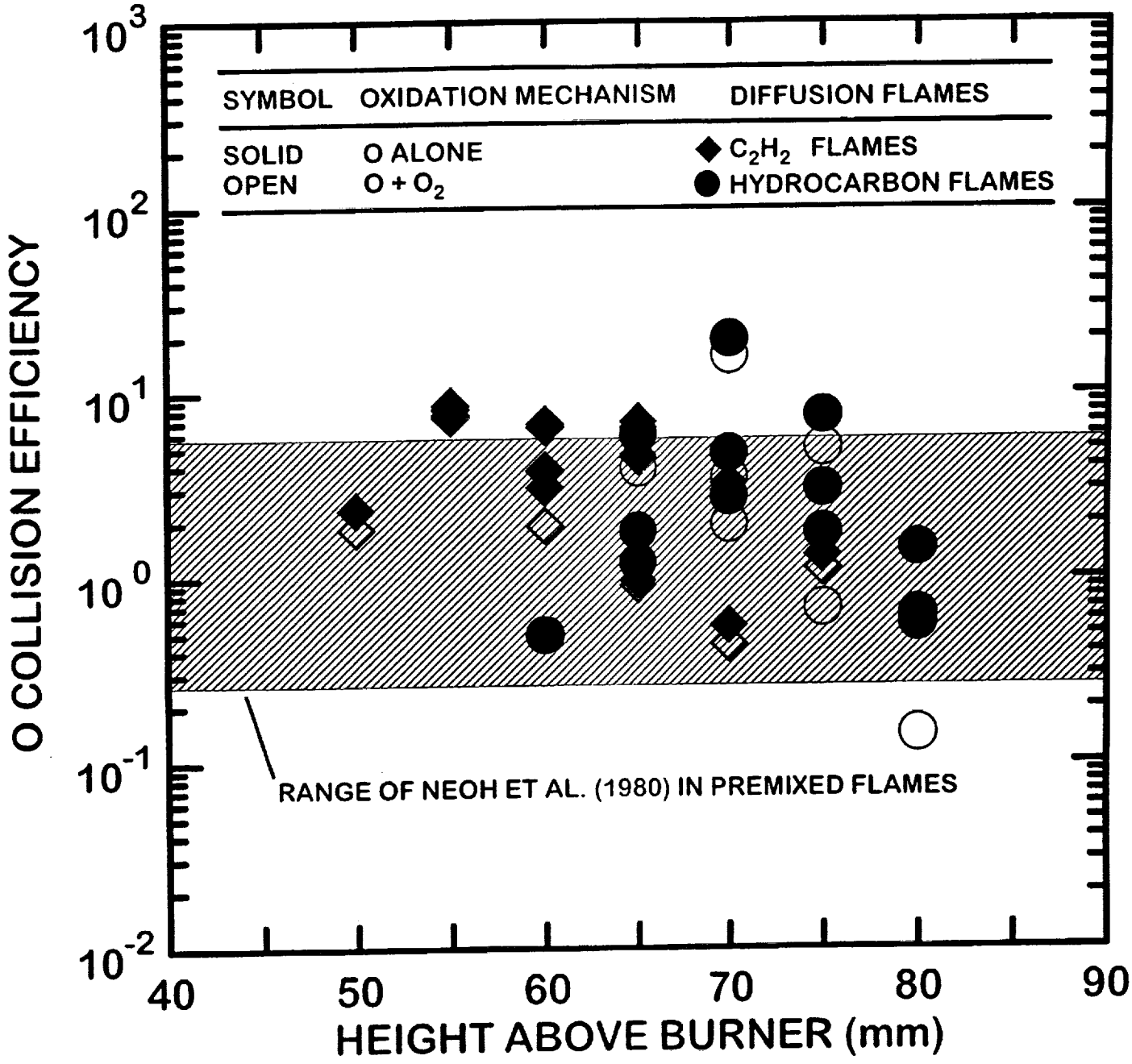
SYMBOL OXIDATION MECHANISM DIFFUSION FLAMES
SOLID O ALONE
OPEN O + O_2
C_2H_2 FLAMES
HYDROCARBON FLAMES
RANGE OF NEOH ET AL. (1980) IN PREMIXED FLAMES
O COLLISION EFFICIENCY
10^3
10^2
10^1
10^0
10^{-1}
10^{-2}
40
50
60
70
80
90
HEIGHT ABOVE BURNER (mm)

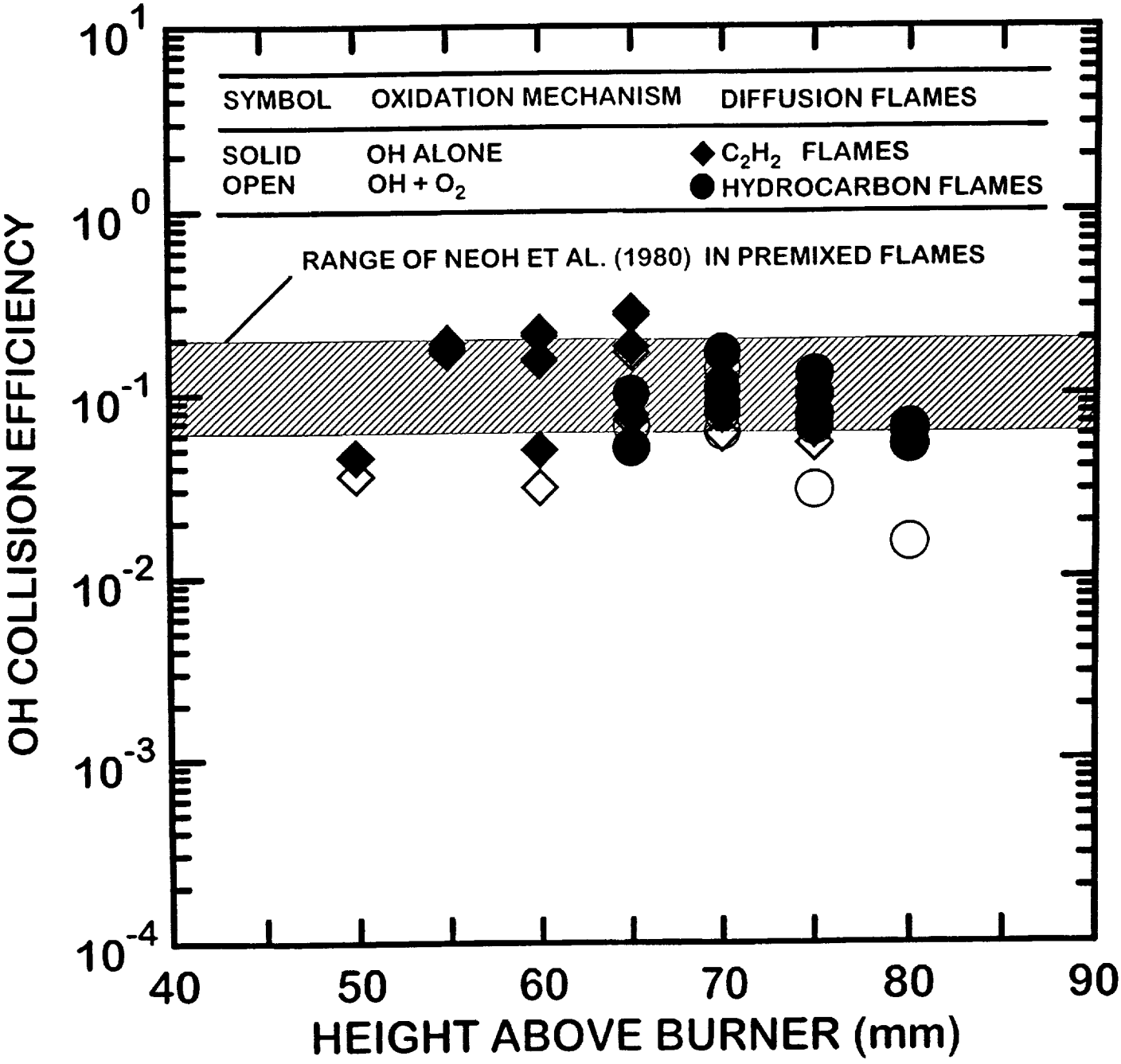
SYMBOL OXIDATION MECHANISM DIFFUSION FLAMES
SOLID OH ALONE
OPEN OH + O2
C2H2 FLAMES
HYDROCARBON FLAMES
RANGE OF NEOH ET AL. (1980) IN PREMIXED FLAMES
OH COLLISION EFFICIENCY
10^1
10^0
10^-1
10^-2
10^-3
10^-4
40
50
60
70
80
90
HEIGHT ABOVE BURNER (mm)

(b)